Automated Gain Control Ion Funnel Trap for Orthogonal Time-of-Flight Mass Spectrometry

4 AUTHORS:

Yehia M Ibrahim
Pacific Northwest National Laboratory
72 PUBLICATIONS **643** CITATIONS

SEE PROFILE

Mikhail Belov
Pacific Northwest National Laboratory
50 PUBLICATIONS **1,363** CITATIONS

SEE PROFILE

Andrei V Liyu
Pacific Northwest National Laboratory
6 PUBLICATIONS **59** CITATIONS

SEE PROFILE

Richard D Smith
Pacific Northwest National Laboratory
1,131 PUBLICATIONS **45,976** CITATIONS

SEE PROFILE

Automated Gain Control Ion Funnel Trap for Orthogonal Time-of-Flight Mass Spectrometry

Yehia M. Ibrahim, **Mikhail E. Belov**[*], **Andrei V. Liyu**, and **Richard D. Smith**
Biological Sciences Division, Pacific Northwest National Laboratory, P.O. Box 999, Richland, Washington 99352

Abstract

Time-of-flight mass spectrometry (TOF MS) is increasingly used in proteomics research. Herein, we report on the development and characterization of a TOF MS instrument with improved sensitivity equipped with an electrodynamic ion funnel trap (IFT) that employs an automated gain control (AGC) capability. The IFT-TOF MS was coupled to a reversed-phase capillary liquid chromatography (RPLC) separation and evaluated in experiments with complex proteolytic digests. When applied to a global tryptic digest of *Shewanella oneidensis* proteins, an order-of-magnitude increase in sensitivity compared to that of the conventional continuous mode of operation was achieved due to efficient ion accumulation prior to TOF MS analysis. As a result of this sensitivity improvement and related improvement in mass measurement accuracy, the number of unique peptides identified in the AGC-IFT mode was 5-fold greater than that obtained in the continuous mode.

Hybrid instruments, such as ion trap time-of-flight (IT-TOF) mass spectrometers, have become indispensable tools for analyzing and characterizing a variety of biomolecules.[1,2] The orthogonal acceleration TOF (oa-TOF) constitutes the core of these systems due to its high throughput, mass resolving power, mass measurement accuracy, and sensitivity.[3,4] Radio frequency (rf) ion guides (e.g., quadrupoles) have successfully been used to couple continuous ion sources, such as electrospray ionization (ESI), with TOF mass spectrometers.[5] The collisional cooling in the rf ion guides helps minimize the initial radial velocity spread of ions introduced into the oa-TOF extraction region and improves resolution.[6]

High sensitivity is vital for use of a TOF instrument in biochemical research. At low number of ion counts, M, the probability of detection is determined by the Poisson statistics. If measurement is repeated a large number of times and the values of M counts are averaged, the averaged value of M approaches the mean of the distribution. Under the assumption of zero background, the signal-to-noise ratio (S/N) can be determined as follows. The uncertainty of a measurement, also described as the standard deviation of Poisson distribution, $\sigma_N \cong \sqrt{M}$, will define the "noise". The "signal" will be determined by the mean of the Poisson distribution, M. Therefore, the S/N will be governed by $S/N = \sqrt{M}$. Given that S/N is proportional to the square root of the duty cycle, which is proportional to the number of detected ions,[7] improving the latter expands the range of TOF mass spectrometry (MS) applications. For example, rf guides have been used as storage devices to improve the instrument duty cycle by synchronizing the release of stored ion populations with the TOF extraction pulse.[8,9] However, these improvements in the duty cycle were obtained at the expense of the detectable m/z range, which imposed the need to use a set of delays between the ion release and TOF extraction pulses to cover a broad m/z range.[8] Alternatively, ion utilization efficiency has been enhanced

* To whom correspondence should be addressed. E-mail: E-mail: mikhail.belov@pnl.gov..

by multiplexing ion packet introduction into the TOF flight tube via TOF pulser encoding with a maximum-length pseudorandom sequence.[10] Although the use of gridless ion mirrors has reduced ion losses[11-13] and enhanced TOF MS sensitivity, further TOF MS design improvements will offer diminishing return. However, a significant improvement in sensitivity is expected to be obtained with a "brighter" ion source.[14] The use of a brighter ion source would present a challenge for rf ion guides and the TOF MS in terms of undesirable space-charge effects. Additionally, increased ion populations in rf ion guides are known to induce m/z errors, discriminate against high m/z ions, or cause instabilities for lower m/z ions[15,16] and, in some cases, induce fragmentation.[17]

Increased space charge in the TOF extraction region gives rise to a broader initial radial velocity distribution and also causes detector saturation that leads to reduced mass resolution and degraded quantitation. To counteract the space-charge effect in the continuous mode of operation, data-directed throttling of the ion beam has been proposed to reduce the number of ions and avoid detector saturation.[18] For an ion trap coupled to a dynamic ion source, such as from reversed-phase capillary liquid chromatography (RPLC) separation, the accumulation of the optimum number of ions in the trap has been implemented with automated gain control (AGC). In this approach, the accumulation time is adjusted according to the flux of the incoming ion beam to ensure nearly constant ion populations are accumulated in the trap in spite of significant variations in the ion production rates.[19-21] In IT MS operation, the incoming ion beam density is determined by the AGC prescan which is composed of a short fixed accumulation event followed by a rapid mass-selective detection of the trapped ions. In a hybrid IT-TOF MS, the AGC prescan can be carried out with a TOF detector while the ion trap operates in transmission, rather than trapping, mode. Taking advantage of the fast TOF MS data acquisition rates, the prescan can thus be accomplished faster than a mass-selective scan with the ion trap. In addition, an AGC prescan conducted with IT-TOF MS is unlikely to suffer m/z discrimination from high ion populations, since it is conducted in the transmission mode.

We have recently shown that the use of an ion funnel trap (IFT) operating at ~1 Torr resulted in more than order-of-magnitude improvement in the TOF MS S/N and limit of detection (LOD).[22] Ion current measurements indicated that the amplitude of an ion pulse from the trap exceeded that of the continuous ion beam by more than 2 orders of magnitude. These improvements in instrument sensitivity were reported for well-controlled ion populations in the IFT. Given the practical challenge associated with inherent large variations in ion currents encountered from RPLC separations, it is important to maintain ion populations in the IFT below the space-charge level that causes a decline in TOF mass resolution and mass accuracy. In this study, we addressed this challenge by implementing an AGC capability that increased instrument sensitivity and dynamic range, while exhibiting similar mass resolution and mass measurement accuracy compared to that obtained in the continuous mode. Herein we report on the development and evaluation of an IFT-TOF MS instrument with AGC-trapping capability. Instrument performance was investigated over the course of RPLC separations using bovine serum albumin and *Shewanella oneidensis* tryptic digests.

EXPERIMENTAL SETUP

The design (Figure 1a) of our IFT-TOF MS has been described elsewhere;[22] therefore, only the details relevant to the current setup are presented here. Ions were formed by positive mode ESI and transmitted to the MS through a dual-channel 508 μm i.d., 20 cm long steel inlet capillary interface heated to ~165 °C. The two separate inlet capillaries were used to introduce analyte and calibrant ions, respectively. Ions exiting from the heated capillaries merged into an electrodynamic ion funnel and focused at the bottom of the funnel before entering an ion trap to be either transmitted continuously (continuous mode) or accumulated and stored using

a predetermined time sequence (trapping mode). The pressure in the funnel and the trap was ~1.3 Torr. The ions exiting the IFT were captured by a collision quadrupole and transmitted first into a selection quadrupole and then into an oa-TOF MS equipped with a dual-stage reflectron. Both collisional and selection quadrupoles were powered using a custom-made rf drive at a frequency of 2 MHz and an rf amplitude of 2.5 kV_{pp}. The TOF MS has a maximum mass resolving power of 10 000 and a repetition rate of 10 kHz. The TOF has 40 mm diameter extended dynamic range bipolar detector (Burle ElectroOptics, Sturbridge, MA) which was impedance-matched to a 2 GS/s 8-bit analog-to-digital converter AP200 (Acqiris, Geneva, Switzerland).

The electrodynamic ion funnel (Figure 1b, sections 1–2) and the IFT (Figure 1b, sections 3–5) consisted of 98 brass ring-electrodes that were 0.5 mm thick, of variable inner diameters, and separated by 0.5 mm thick Teflon spacers. The trapping volume in section 4 is separated from sections 3 and 5 by the entrance and exit grids, respectively. The two grids were made of 95% transmission electroformed nickel mesh (InterNet Inc., Minneapolis, MN). A 180° phase-shifted rf was applied to the electrodes adjacent to the funnel and IFT. A controllable dc gradient was created through a resistor chain and superimposed onto the rf field to assist ion transmission through the funnel and IFT. The resistor and capacitor chains were mounted on separate printed circuit boards, which were then attached to the funnel through custom-made zero insertion force connectors (Tactic Electronics, Plano, TX).

The rf field applied to the device generated an effective potential that confined ions radially, while axial confinement in the IFT region was established by applying appropriate potentials to the grids. The applied dc gradient and the rf frequency and amplitude as well were varied depending on the sections of funnel trap and the operation mode. The dc gradient was 20 V/cm in sections 1–3 and 5, and 4 V/cm in section 4. Lowering the dc gradient in the trap region from 20 to 4 V/cm was found to significantly improve ion-trapping efficiency.[22] This dc gradient profile was applied in the continuous mode, while additional potentials were applied in the trapping mode to the entrance and exit grids to admit, store, and eject ions from the trap. A 6.4 mm brass disk (jet disruptor) was placed ~20 mm at the funnel entrance to minimize gas dynamics and introduction of neutrals into the trap and mass spectrometer.[23] An independent dc voltage (~−25 V offset from the funnel entrance dc voltage) was applied to the jet disruptor.

Automated Gain Control

An AGC capability was implemented to control the number of ions created following the RPLC separation and admitted to the IFT. The computer-controlled timing for the AGC-IFT-TOF MS experiments was determined by a PCI board NI-6532 (National Instruments, Austin, TX), and the amplitude of the analog waveform was set by a PCI board NI-6713. The experimental sequence was uploaded to a custom-made sequencer that provided a temporal resolution of 1 μs in "raster" mode. The time sequence for the AGC mode and the trap pulsing sequence is shown in Figure 1c. The AGC sequence is divided into prescan and full scan elements; however, neither the trap nor the TOF were scanned, and the term "scan" is used in analogy with ion traps. In the prescan, the ions were introduced continuously (no trapping) for 100 ms into the TOF to determine the total ion count (TIC), where the TIC is the sum of intensities in all TOF bins for the m/z range of interest. The prescan TIC was calculated for all ion intensities above a user-defined threshold that corresponded to the baseline noise.

The full scan consisted of multiple accumulation–storage–ejection cycles in the trap referred to as "miniscans" (Figure 1c). On the basis of the prescan TIC, the trap accumulation time (t_{accm}) was determined as

$$t_{\text{accm}} = \frac{A}{\text{prescan TIC}}$$

(1)

where A is a coefficient that determines the target number of ions to be accumulated. The accumulation time (to a maximum preset value) determined how long the entrance grid should stay open to admit ions into the trap while the exit grid was closed. Following the accumulation event, ions could be stored by raising the potential on the entrance and exit grids. However, the ion storage option was not used in this work. It is noteworthy that no detectable ion accumulation signal could be recorded when trapping ions in the region preceding the entrance trapping grid, presumably due to the diverging geometry of section 3 (see Figure 1b) that causes ion losses on the funnel electrodes. The ions were then ejected from the trap in 108 μs by lowering the potential on the exit grid, while maintaining a high potential on the entrance grid to ensure that only the trapped ions were being ejected. The length of time for each accumulation, storage, and ejection event was a multiple of 108 μs (the TOF extraction time) to reduce delays in uploading the experimental sequence. The miniscan was repeated for the duration of the TOF acquisition period, which was typically set to 1 s followed by data transfer (~20 ms). The TOF acquisition time was set to 3 s for an LC–MS experiment to reduce the data file size (~900 MB for 60 min LC–MS experiment). The AGC cycle was then repeated for the entire RPLC–MS analysis. The TOF extraction pulse did not need to be synchronized with the IFT ion release pulse because of the relatively broad temporal profile of ion packets arriving at the TOF extraction region [~1–2 ms fwhm (full width at half maximum)].[22] Note that since the TOF acquisition time was fixed to 1 s (or 3 s) and the miniscan duration varied depending on the accumulation time, the number of miniscans/s also varied. As the accumulation time increased, the number of miniscans/s decreased and vice versa.

LC Parameters

RPLC separations were performed using a fully automated two-column system.[24] The separation was conducted under a constant pressure of 5000 psi, using 150 μm i.d. fused-silica columns packed with 5 μm bonded C-18 particles (Phenomenex, Torrance, CA), which resulted in a capillary flow rate of ~2 μL/min. Mobile phase A was prepared from purified water acidified with 0.20% acetic acid and 0.05% trifluoroacetic acid, and mobile phase B was 90% acetonitrile acidified with 0.10% trifluoroacetic acid. The sample loop volume was 10 μL, and the LC gradient was ramped linearly over 60 min. MS acquisition was triggered using a contact closure 10 min after the start of the gradient.

Chemicals and solvents were purchased from Sigma-Aldrich (Sigma-Aldrich, St. Louis, MO) and used without further purification. Samples for direct infusion were prepared in 50% aqueous methanol acidified with 1% acetic acid.

Sample Preparation

Proteolytic digestions of bovine serum albumin (BSA; Pierce Biotechnology, Rockford, IL) were conducted using sequencing grade trypsin (Promega, Madison, WI) and a previously described procedures.[25] The *S. oneidensis* tryptic digest was prepared as reported previously. [26]

Data Analysis

LC–MS data sets were analyzed using the accurate mass and time (AMT) tag approach. Briefly, accurate mass and elution time features were matched to those in a peptide database generated previously from numerous "shotgun" LC–MS/MS analyses. Information for each peptide in the AMT tag database included peptide sequence, mass, and LC elution time, in addition to

other parameters. Peptide signals in LC–MS spectra were "deisotoped" using Decon2LS software developed in-house to determine species' charge states and corresponding neutral masses.[27] The list of neutral masses and elution times was used to construct a two-dimensional (2D) map,[28] and the data were clustered according to neutral mass deviation (within a predetermined mass accuracy) and elution profile continuity. Clustered data were then aligned in elution time and mass domains to corresponding entries in the AMT tag database to obtain the best fit to the database.[27] Features that fit within alignment criteria were searched against peptide identifications within a user-defined mass accuracy and predicted normalized elution time. Identified peptides were filtered to remove redundant identifications, resulting in a list of "unique" peptides.

RESULTS AND DISCUSSION

The effect of space charge accumulated in the IFT on oa-TOF MS mass resolution was systematically studied using a number of analytes. Ion populations in the IFT were varied by modulating the reserpine ion beam introduced into the trap. The ion beam was modulated by varying the voltage applied to the jet disruptor (Figure 1b).[29] The study was performed at a constant IFT accumulation time of 21.6 ms and an ejection time of 108 μs. Figure 2a shows the TIC (total ion counts per spectrum) for a modulated ESI ion beam of 1 μM reserpine and the mass resolving power of the reserpine monoisotopic peak as a function of the scan number. Note that as the TIC increases, the TOF mass resolving power decreases correspondingly. At the maximum TIC value, the TOF mass resolving power declined to ~50% of its optimum value. Additional experiments revealed no dependence of IFT storage time on mass resolving power (data not shown). Since the ion packet density that exited the trap was 2 orders of magnitude higher than that of the continuous beam,[22] the ion packet dispersion due to the increased space-charge effect in the TOF extraction region resulted in a broadening of the ion's initial velocity distribution (prior to extraction) along the TOF axis and a longer "turnaround" time, which leads to a decrease in mass resolving power.[30] Figure 2b shows the dependence of the TOF mass resolving power as a function of the TIC for the data presented in Figure 2a. Data obtained in the continuous mode are also shown in Figure 2b for comparison. Note that, as the number of ions increase, the TOF mass resolving power decreases accordingly. The degradation of resolution for the trapping mode was observed to be more pronounced than that observed in the continuous mode, which we attribute to a greater space-charge effect.

To improve TOF mass resolving power and concurrently maintain high sensitivity, the number of ions ejected from the trap needs to be reduced while the number of IFT release pulses is proportionally increased. Importantly, the number of ions in the TOF extraction region just prior to an extraction pulse should not exceed the space-charge limit that causes degradation in mass resolving power. As previously demonstrated with IT MS,[31] the AGC capability enables dynamic adjustments of ion accumulation times according to the incoming ion flux for systems with signal variability of greater than 3 orders of magnitude (e.g., LC separation). In the case of IFT-TOF MS, an AGC prescan can be performed with TOF MS operating in the continuous mode to minimize the discrimination effects observed in ion traps at higher incoming ion currents. In addition, fast data acquisition rates of the TOF MS allow the prescan time to be shortened to below 100 ms.

The initial evaluation of the AGC capability was conducted using a BSA tryptic digest and on-line RPLC coupled to the IFTTOF MS operating in both continuous and AGC-trapping modes. Figure 3a shows the inverse of the IFT accumulation time as a function of the scan number/ separation time. Parts b and c of Figure 3 demonstrate the TIC chromatograms of the AGC prescan and full scan. The TIC chromatogram of a typical RPLC separation in the continuous mode is shown in Figure 3d for comparison. The results in Figure 3, parts a and b, indicate that variations in the prescan intensity were effectively tracked by the IFT accumulation time. Note

that the maximum accumulation period was preset to 54 ms to limit the accumulation time in instances when no useful signals (such as those in LC separation valleys) were detected. Parts b and c of Figure 3 show that a full scan TIC followed the prescan TIC, which indicates successful implementation of the AGC capability. Importantly, no TIC adjustment (for variable accumulation time) was necessary because of the fixed TOF data acquisition period that allowed the number of miniscans to vary. An increase in the ion accumulation time results in an increase in the number of ions to the AGC target value. However, the number of trap releases per TOF acquisition time decreases. The net result is that AGC-adjusted TIC tracks the prescan TIC. In traditional AGC used in commercial ion traps, the number of scans per spectrum acquisition is fixed, while the injection time varies as a function of the incoming ion current. Therefore, to obtain raw signal intensities, the acquired TIC needs to be rescaled to account for change in the injection time. Comparison with the continuous mode (Figure 3d) shows almost identical TIC chromatograms with no reduction in either separation peak capacity or skewing of the relative peaks intensities due to the ion trapping or AGC prescan step. Furthermore, the TOF mass resolving power did not degrade for high-abundance peptide peaks.

The effect of peptide peak intensity on mass resolving power is shown in Figure 4. The mass resolving power of the eluted monoisotopic peak for the highly abundant peptides AEMKASEDLKK, KVPQVSTPTLVEVSR, and KQTALVELLK is shown for both continuous and AGC-trapping modes. Contrary to the trends in Figure 2, the mass resolving power did not decline as signal intensities increased and appeared similar to that observed in the continuous mode. Data analysis of the RPLC–MS experiment in Figure 3c resulted in 110 unique peptides within a mass measurement accuracy of 10 ppm, which represents BSA amino acid sequence coverage of 81%.

Despite successful implementation of the AGC capability, the results shown in Figure 3 revealed no sensitivity gain in the AGC-trapping mode compared to that in the continuous mode. This observation corroborates the finding that the signals produced by 0.1 μg/μL BSA tryptic digest were such that for the majority of the peptide peaks, the ion accumulation time needed to be reduced by 2 orders of magnitude (see Figure 3a) to avoid detrimental space-charge effects in the TOF extraction region. Therefore, in accord with our previous report,[22] no sensitivity improvement due to ion trapping could be attained for higher concentration samples. To realize the benefit of the ion-trapping capability augmented with AGC, we evaluated a global tryptic digest of *S. oneidensis* at concentrations that ranged from 0.30–0.05 μg/μL. Similar to the BSA study, analyses of higher concentration samples did not benefit from the ion-trapping mode and yielded comparable numbers of peptide identifications as those obtained in the continuous mode. However, data obtained for the lowest sample concentration of 0.05 μg/μL (0.5 μg sample loaded onto the LC column) were in stark contrast to the higher concentration data. Figure 5a compares base peak chromatograms of 0.05 μg/μL *S. oneidensis* tryptic digest recorded in continuous and AGC-trapping modes. It is evident that at least an order-of-magnitude improvement in base peak intensity (BPI) was obtained due to AGC ion trapping. The data presented in Figure 5a were further analyzed to quantify the effect of the AGC-trapping mode on the number of identified peptides. Figure 5b shows portions of mass spectra for two peptides identified in both AGC-trapping and continuous modes. For the peptide KKQEDVGSIQFANDSAVVK at *m/z* of 688.3696, the peak intensity and S/N are an order-of-magnitude higher in AGC-trapping mode than that in the continuous mode. For the low-intensity peaks, such as the peptide DFNEALVHQVVVAYAANAR at *m/z* of 696.3621, the isotopic distribution was identified and converted to the neutral mass based on the charge state information, whereas the signal recorded in the continuous mode could not be "deisotoped". We would emphasize that signal improvements for the low-abundance peptides from a complex sample are constrained by the coeluting high-abundance species that determine the prescan TIC. Lower gain observed for the peak at *m/z* of 696.3621 in Figure 5b is an example of this limitation.

The performance improvement due to AGC trapping is also reflected in the number of uniquely identified peptides. Figure 6 shows a 2D display of neutral monoisotopic mass versus scan number for peptides identified using RPLC–MS in AGC-trapping (Figure 6a) and continuous (Figure 6b) modes. The charge states of the peptides used to obtain the neutral monoisotopic mass are also shown. The difference in the number of identified peptides between the AGC-trapping and the conventional continuous modes is readily apparent; 73 peptides were confidently identified in the continuous mode, whereas 383 peptides were confidently identified in the AGC-trapping mode, i.e., an ~5-fold improvement.

The mass measurement accuracy for the data in Figure 6 is presented in Figure 7 along with a Gaussian fit to the data. The error histogram in Figure 7 is centered at zero ppm and spans a width of ~18 ppm (at fwhm). For comparison, Figure 7b shows the error histogram for the data acquired in the continuous mode. Although the histograms in Figure 7, parts a and b, have similar widths, the comparison indicates an improvement in the number of identified peptides (i.e., distribution height) in the AGC-trapping mode. The peptides identified in AGC-trapping and continuous modes along with their mass measurement accuracy are listed in Table 1. The AGC-assisted ion trapping prior to TOF MS analysis consistently improved analytical sensitivity for detecting low-concentration peptides from complex proteolytic digests. All species were efficiently ejected from the IFT in an ~100 μs pulse,[22] which implies no discrimination effect due to gas phase separation in the IFT prior to ejection.

Although the reported experimental observations were highly reproducible, consistent explanation of the observed effects has been challenging. As presented above, system performance with higher concentration samples was similar in both continuous and trapping modes, implying comparable S/N and chemical background levels. If ion losses at lower ion abundances were the same in the continuous and ion-trapping modes, one would not observe the S/N and signal improvements due to the ion trapping at low concentrations. Therefore, we attempted to discern nonlinear ion focusing effects that are responsible for different rates of signal decrease at low concentrations (or ion abundances) in the two modes of operation. In addition, enhanced droplet desolvation in the ion funnel was investigated as a potential contributor to the increased S/N in the trapping mode. To isolate effects pertinent to the ion optics, a 1 μM neurotensin solution was directly infused into the instrument and the ESI-generated ion currents were attenuated by varying the jet disruptor potential. Higher concentration analyte solution was used to minimize chemical background contribution to the overall detected signal and to concurrently perform data acquisition at a low number of ion counts. Similar to the earlier reported results obtained with lower concentration samples (e.g., Figure 3 in ref [22]), the S/N of the triply protonated neurotensin detected in the trapping mode was found to exceed that recorded in the continuous mode by an order of magnitude. Initially, total ion current measurements were conducted in the two modes of operation using the collisional quadrupole as a charge collector. It was found that the ratio of the total number of charges in the continuous and trapping modes detected over an accumulation period of 10.8 ms was reduced by a factor of ~1.5 at a 10-fold decrease in the incoming ion current that only partially explains the observed S/N enhancement due to the trapping. We attribute this effect to inefficient ion trapping in the shallow axial wells at the exit of the ion funnel.[32] An increase in the charge density of an ion cloud, as observed in the trapping mode, results in rapid saturation of these axial wells and improved ion transmission. In the following set of experiments, the ion currents were investigated as a function of the jet disruptor voltage (i.e., ESI-generated ion current) using the Faraday cup charge collector positioned downstream of the TOF extraction region. Figure 8a shows comparison of the signals observed at a jet disruptor bias of 290 V that caused efficient beam throttling. Whereas ~0.1 ± 0.1 pA continuous ion current was detected (practically immeasurable signal as compared to the baseline), the amplitude of the pulsed ion current exceeded 30 pA, which corresponds to the number of ions accumulated in the trap over a period of 756 ms. Figure 8b depicts the dependences of the total

number of ions, N_total, at the charge collector on the jet disruptor voltage for both continuous and trapping modes. As seen in the graph, the rates of ion loss in the continuous and trapping modes are different, causing the two dependences to intersect at the total of number of ions of $\sim 4 \times 10^5$. In the employed TOF instrument, the kinetic energy of ions entering the 40 mm long TOF extraction region is 5 eV. Therefore, ion species at m/z 500 traverse the TOF extraction region in $\sim 30\,\mu s$. Limited by the ion losses on the grids, TOF transmission efficiency, including detector conversion efficiency, is $\sim$ 10%. Given all the observed ions are due to the triply protonated neurotensin (that is an overestimate), 4×10^5 ions detected at the charge collector over 756 ms period would yield single ion strikes per TOF scan at the TOF detector [(4 × 10^5/756)(0.03)(0.1) $\sim$ 1.6]. Therefore, if probability of ion detection per TOF scan were less than unity in the continuous ion mode (that corresponds to the jet disruptor bias of >270 V in Figure 8b), the ion-trapping mode is expected to deliver greater number of ions to the TOF analyzer and consequently provide higher signal intensities. Though experimental observations point to the different rates of ion losses between the ion funnel exit and the TOF extractor region at the low number of ions, the actual mechanism needs explanation. We would argue that the different rates of ion losses at the low number of ions in the continuous and trapping modes are due to the ion defocusing in the fringing rf field between the ion funnel and collisional quadrupole. An ion cloud collimated in the ion funnel assumes a donut-like shape, with the charge density exponentially increasing at the electrode edges.[32,33] If such an ion cloud enters a 1 mm gap between the ion funnel and the quadrupole operating at an rf amplitude of 2.5 kV$_{pp}$, ions at the periphery of the ion cloud would experience a strong defocusing field and be dispersed beyond the quadrupole acceptance radius. An increase in the ion cloud density due to the bunching effect in the IFT brings about an increase in the ion population on the funnel axis at the exit electrode and improves transmission through the quadrupole rf fringing field. This hypothesis has been verified with SIMION 8.0 modeling. Figure 9 shows the number of ions injected into the collisional quadrupole as a function of the ions' radial position. As seen in Figure 9, the number of transmitted ions decreases rapidly with an increase in the ion's radial position to 1.2–1.5 mm, consistent with the experimental observations. Therefore, we conclude that, at low concentrations, bunching of ions in the IFT increases the charge density on the funnel axis at the last electrode and improves transmission through the funnel– quadrupole interface. Finally, we have evaluated the desolvation effect on the observed S/N improvement. The inlet capillary temperature was varied from 164 to 50 °C, and the signals from both 10 and 100 nM neurotensin solutions were monitored. Figure 10 shows the dependence of the peptide intensity on the inlet capillary temperature along with the three mass spectra at the inlet capillary temperatures of 164, 106, and 50 °C. Unlike the conventional jet– skimmer interface that was reported to have a strong dependence on the inlet capillary temperature causing water clustering and signal degradation at low temperatures,[34,35] the ion funnel interface was found to produce very efficient desolvation due to collisional activation in the funnel region, exhibiting only a weak dependence on the inlet capillary temperature. Though the detailed study of droplet desolvation in the IFT is beyond the scope of this manuscript, Figure 10 provides some evidence that droplet desolvation in the funnel interface is equally efficient in both continuous and trapping modes and is unlikely to be the primary reason for the increased signals at low concentrations in the trapping mode. We would emphasize that further studies are needed to better understand the contribution of droplet desolvation to the reduction of background chemical noise. This feature is characteristic of the ion funnel trapping and has been demonstrated to drastically improve S/N of low-concentration analytes.[22]

Coupling the ion funnel to a mass spectrometer was shown to increase the instrument sensitivity.[36] In this work, we have further advanced the ion funnel capability by developing an AGC-augmented ion trapping in conjunction with TOF MS detection. Higher ion transmission through the elevated pressure regions and reduced chemical background level in

the trapping mode make the IFT-TOF MS instrument an attractive platform for rapid and accurate analysis of low-concentration complex samples in biochemical applications.

CONCLUSIONS

Implementation of an AGC-trapping capability with IFT-TOF MS eliminated undesirable space-charge effects on TOF MS performance. No rescaling of the full scan raw data was required to obtain reliable quantitation due to the fixed TOF acquisition time that allowed the number of miniscans to vary as the accumulation time was adjusted. Importantly, the TOF resolution remained optimal in the AGC-trapping mode as the number of ions in the TOF extraction region was reliably reduced to below the space-charge level causing peak broadening, while high sensitivity was maintained. In contrast, the use of a fixed accumulation time resulted in a decrease in mass resolving power due to excessive space charge in the TOF extraction region. Evaluation of the AGC capability with IFT-TOF MS with a global tryptic digest of *S. oneidensis* bacterial proteome indicated that the sensitivity of the LC–TOF MS instrument was increased by an order of magnitude when sample size was limited. Additionally, the number of peptides identified was increased by a factor of 5 using the AGC-trapping mode compared to the continuous mode. Overall, the IFT-TOF MS with AGC capability enables improved sensitivity, mass resolving power, and mass measurement accuracy and is expected to further enhance MS capabilities in proteomics and other areas of biomedical research.

ACKNOWLEDGMENT

References

1. Marchese S, Gentili A, Perret D, D'Ascenzo G, Pastori F. Rapid Commun. Mass Spectrom 2003;17 (9):879–886. [PubMed: 12717759]

2. Steen H, Kuster B, Mann M. J. Mass Spectrom 2001;36(7):782–790. [PubMed: 11473401]

3. Chernushevich IV, Ens W, Standing KG. Anal. Chem 1999:452A–461A. [PubMed: 9949732]

4. Dodonov A, Kozlovsky V, Loboda A, Raznikov V, Sulimenkov I, Tolmachev A, Wollnik AKH. Rapid Commun. Mass Spectrom 1997;11(15):1649–1656. [PubMed: 9364793]

5. Krutchinsky AN, Chernushevich IV, Spicer VL, Ens W, Standing KG. J. Am. Soc. Mass Spectrom 1998;9(6):569–579.

6. Guilhaus M, Selby D, Mlynski V. Mass Spectrom. Rev 2000;19(2):65–107. [PubMed: 10795088]

7. Szumlas AW, Ray SJ, Hieftje GM. Anal. Chem 2006;78(13):4474–4481. [PubMed: 16808456]

8. Chernushevich IV. Eur. J. Mass Spectrom 2000;6:471–479.

9. Hashimoto Y, Hasegawa H, Satake H, Baba T, Waki I. J. Am. Soc. Mass Spectrom 2006;17(12):1669–1674. [PubMed: 16926098]

10. Belov, M.; Fancher, CA.; Foley, P. Multiplexed Orthogonal Time-of-Flight Mass Spectrometer. U.S. Patent 6,900,431. May 31. 2005

11. Schmid RP, Weickhardt C. Int. J. Mass Spectrom 2001;206(3):181–190.

12. Schmidt L, Jungclas H, Fritsch HW, Kohl P. J. Am. Soc. Mass Spectrom 1993;4(10):782–786.

13. Grix R, Kutscher R, Li G, Grüner U, Wollnik H, Matsuda H. Rapid Commun. Mass Spectrom 1988;2 (5):83–85.

14. Kelly RT, Page JS, Tang K, Smith RD. Anal. Chem 2007;79(11):4192–4198. [PubMed: 17472340]

15. Belov ME, Nikolaev EN, Harkewicz R, Masselon CD, Alving K, Smith RD. Int. J. Mass Spectrom 2001;208(1–3):205–225.

16. Tolmachev AV, Udseth HR, Smith RD. Rapid Commun. Mass Spectrom 2000;14(20):1907–1913. [PubMed: 11013419]

17. Sannes-Lowery KA, Hofstadler SA. J. Am. Soc. Mass Spectrom 2000;11(1):1–9. [PubMed: 10631658]

18. Chernushevich, I.; Loboda, A. Dynamic Range Extension for TOF MS with Orthogonal Injection; Presented at the 55th ASMS Conference on Mass Spectrometry and Allied Topics; Indianapolis, IN. 2007.

19. Weber-Grabau, M.; Bradshaw, SC.; Syka, JEP. Method of Increasing the Dynamic Range and Sensitivity of a Quadrupole Ion Trap Mass Spectrometer Operating in the Chemical Ionization Mode. U.S. Patent 4,771,172. Sept 13. 1988

20. Schwartz, JC.; Zhou, X-G.; Bier, ME. Method and Apparatus of Increasing Dynamic Range and Sensitivity of a Mass Spectrometer. U.S. Patent 5,572,022. Nov 5. 1996

21. Hager, JW. Method of Reducing Space Charge in a Linear Ion Trap Mass Spectrometer. U.S. Patent 6,627,876. Sept 30. 2003

22. Ibrahim Y, Belov ME, Tolmachev AV, Prior DC, Smith RD. Anal. Chem 2007;79(20):7845–7852. [PubMed: 17850113]

23. Kim T, Tang K, Udseth HR, Smith RD. Anal. Chem 2001;73(17):4162–4170. [PubMed: 11569805]

24. Livesay EA, Tang K, Taylor BK, Buschbach MA, Hopkins DF, LaMarche BL, Zhao R, Shen Y, Orton DJ, Moore RJ, Kelly RT, Udseth HR, Smith RD. Anal. Chem 2008;80(1):294–302. [PubMed: 18044960]

25. Kinter, MM.; Sherman, NE. Protein Sequencing and Identification Using Tandem Mass Spectrometry. Wiley-Interscience; New York: 2000.

26. Shen Y, Zhang R, Moore RJ, Kim J, Metz TO, Hixson KK, Zhao R, Livesay EA, Udseth HR, Smith RD. Anal. Chem 2005;77(10):3090–3100. [PubMed: 15889897]

27. Zimmer JSD, Monroe ME, Qian W-J, Smith RD. Mass Spectrom. Rev 2006;25(3):450–482. [PubMed: 16429408]

28. Monroe ME, Tolic N, Jaitly N, Shaw JL, Adkins JN, Smith RD. Bioinformatics 2007;23(15):2021–2023. [PubMed: 17545182]

29. Page JS, Bogdanov B, Vilkov AN, Prior DC, Buschbach MA, Tang K, Smith RD. J. Am. Soc. Mass Spectrom 2005;16(2):244–253. [PubMed: 15694774]

30. Dodonov AF, Kozlovski VI, Soulimenkov IV, Raznikov VV. Eur. J. Mass Spectrom 2000;6(6):481–490.

31. Belov ME, Zhang R, Strittmatter EF, Prior DC, Tang K, Smith RD. Anal. Chem 2003;75(16):4195–205. [PubMed: 14632135]

32. Tolmachev AV, Kim T, Udseth HR, Smith RD, Bailey TH, Futrell JH. Int. J. Mass Spectrom. Ion Processes 2001;203:31–47.

33. Gerlich, D. Inhomogeneous RF Fiels: A Versatile Tool for the Study of Processes with Slow Ions. In: Ng, C-Y.; Baer, M., editors. State-Selected and State-to-State Ion–Molecule Reaction Dynamics. Part 1. Experiment. Vol. 82. Wiley; New York: 1992. p. 1-176.

34. Allen MH, Vestal ML. J. Am. Soc. Mass Spectrom 1992;3:18–26.

35. Chowdhury SK, Katta V, Chait BT. Rapid Commun. Mass Spectrom 1990;4(3):81–87. [PubMed: 2134340]

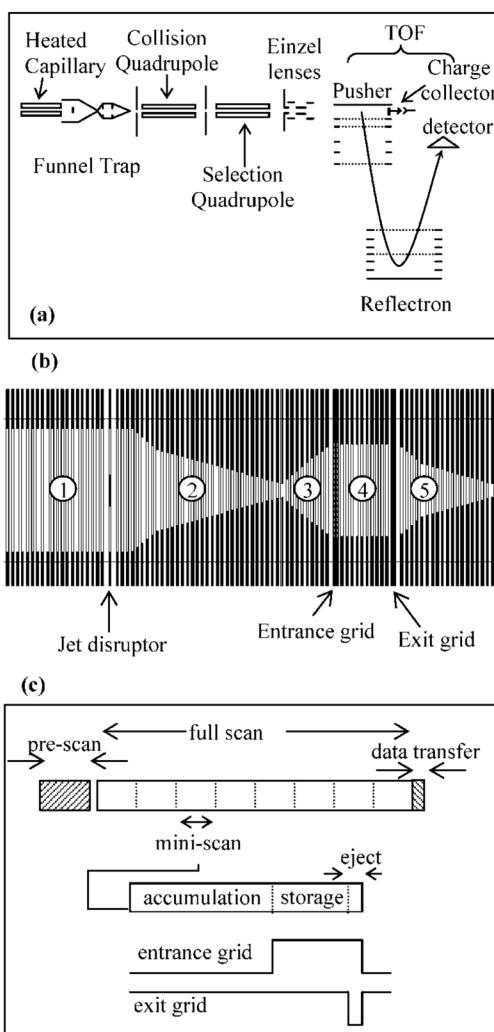36. Shaffer SA, Prior DC, Anderson GA, Udseth HR, Smith RD. Anal. Chem 1998;70(19):4111–4119. [PubMed: 9784749]

Figure 1.
Schematic diagrams of (a) instrument setup, (b) sections of the funnel trap (refer to text for details), and (c) time and pulse sequence for the trap in the AGC mode.
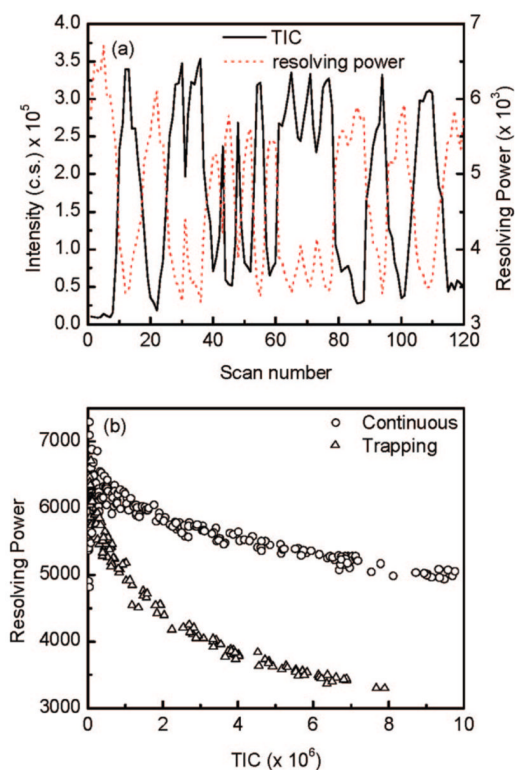
Figure 2.
(a) Reserpine TIC (solid line) and mass resolving power (red dotted line) as function of scan number for 21.6 ms trap accumulation time. (b) The resolving power of reserpine monoisotopic peak as function of TIC for the continuous and trapping mode. The reserpine ion beam was modulated by varying the voltage applied to the jet disruptor.
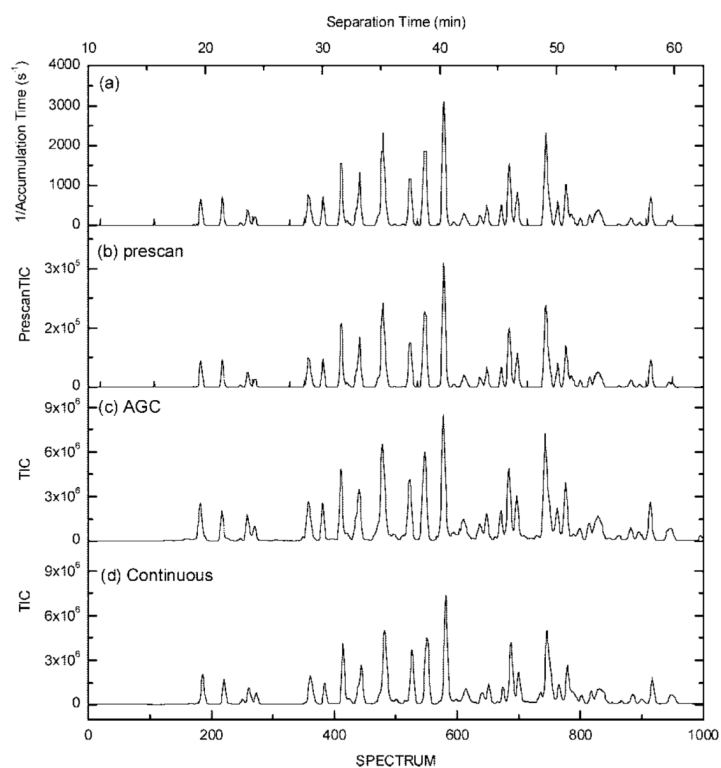
Figure 3.
Reversed-phase LC separation of 0.1 μg/μL BSA tryptic digest using AGC-trapping (panels a–c) and continuous modes (panel d).
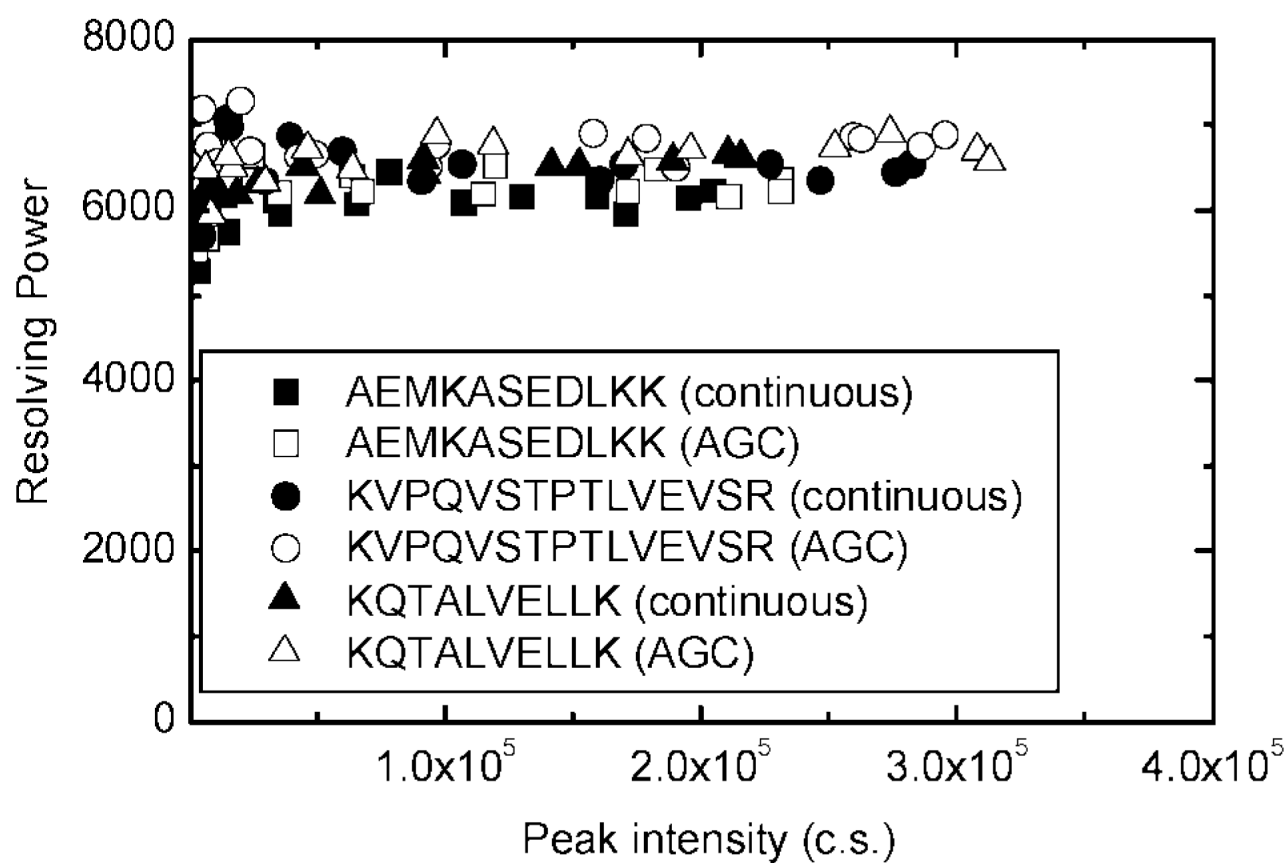
Figure 4.
TOF MS resolving power as a function of the monoisotopic peak intensity for three high-abundant BSA tryptic peptides in the continuous and AGC-trapping modes.
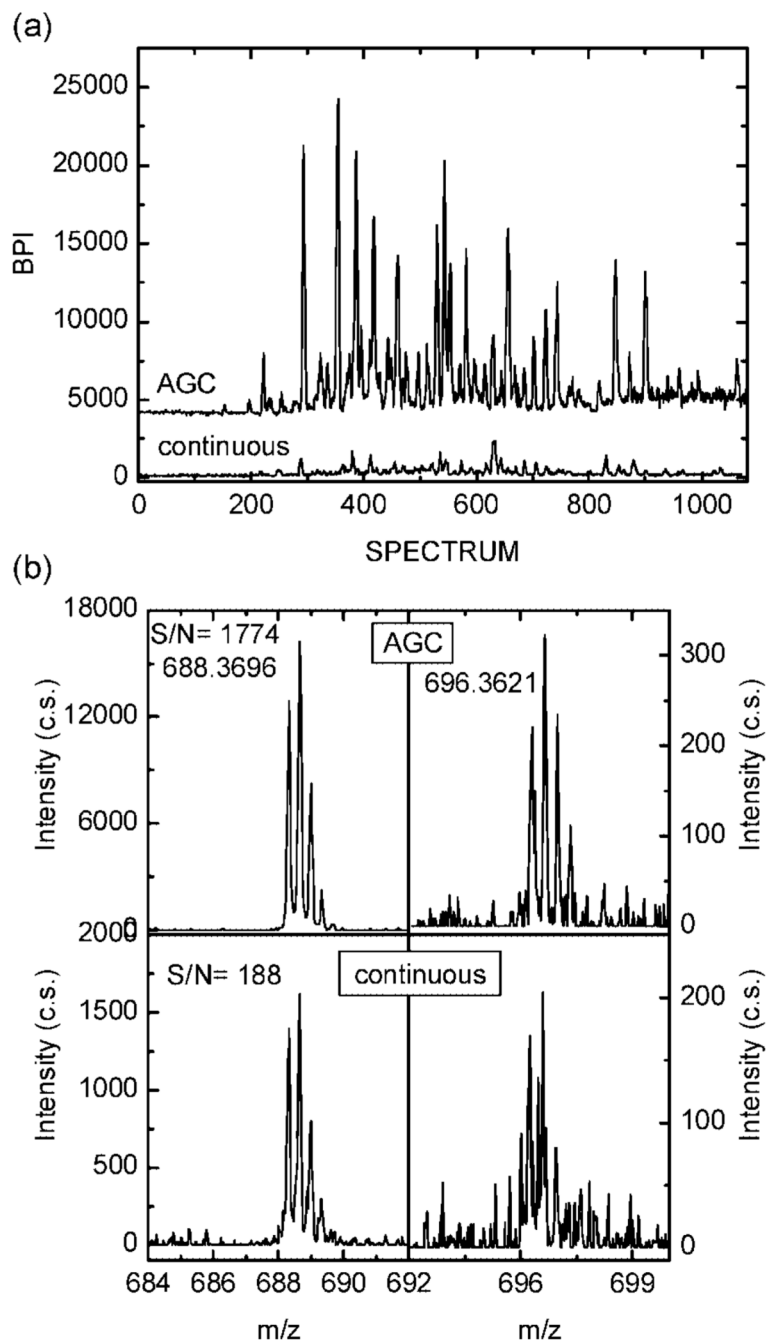
Figure 5.
(a) Base peak intensity (BPI) for the RPLC separation of 0.05 *μg/μL S. oneidensis* tryptic digest in the AGC-trapping and continuous modes. Note that the trace for the AGC-trapping mode is offset for clarity. (b) Segments of mass spectra for KKQEDVGSIQFANDSAVVK (*m/z* 688.3696) and DFNEALVHQVVVAYAANAR (*m/z* 696.3621) peptides from RPLC–MS of 0.05 *μg/μL S. oneidensis* tryptic digest in the AGC-trapping and continuous modes.
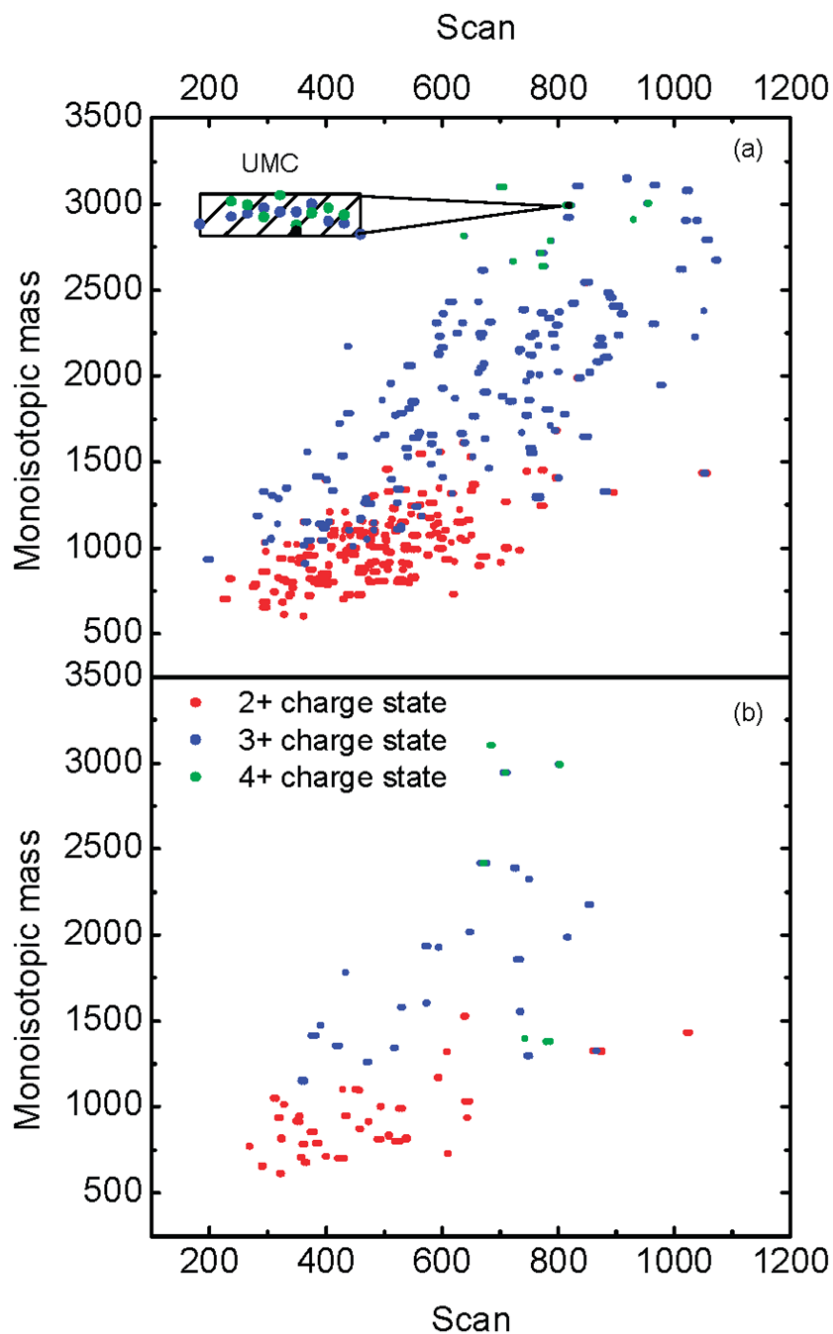
Figure 6.
Two-dimensional (2D) display of the neutral monoisotopic mass vs RPLC scan number for peptides identified from 0.05 μg/μL *S. oneidensis* tryptic digest in (a) AGC-trapping mode and (b) continuous mode. The inset in panel (a) exemplifies data points clustered into a unique mass class.
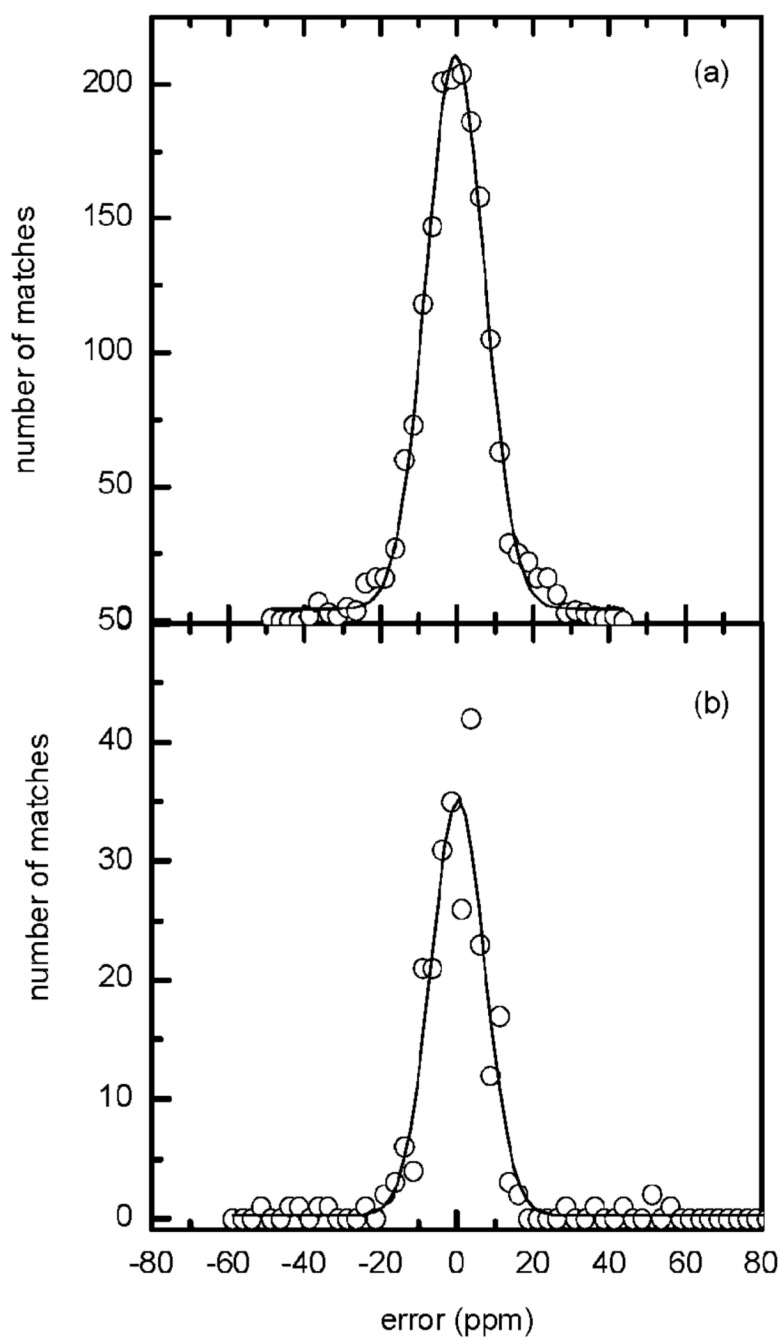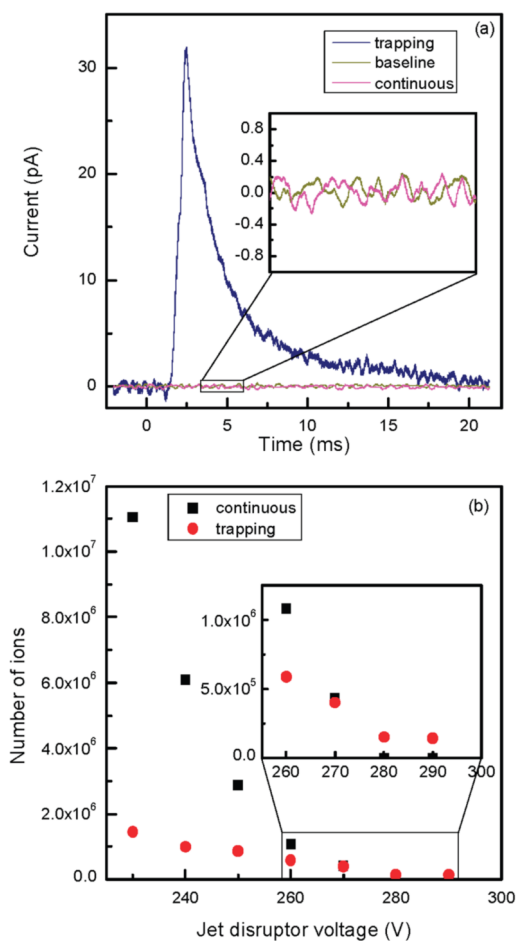
Figure 7.
Mass measurement accuracy histogram (error, ppm) for peptides identified in an RPLC–MS analysis of 0.05 μg/μL *S. oneidensis* tryptic digest in (a) AGC-trapping mode and (b) continuous mode. The solid line represents a Gaussian fit to the data points.

Figure 8.
(a) Representative signals in the continuous and trapping modes (756 ms accumulation time) corresponding to a jet disruptor voltage of 290 V. The inset indicates efficient ion beam throttling. (b) Total number of ions from ESI of 1 μM neurotensin solution impinging at the Faraday cup charge collector in the continuous and trapping modes as a function of jet disruptor voltage. The number of ions in the trapping mode was calculated by integrating the area under the ion pulse (such as the one shown in panel a) while in the continuous mode the charges were calculated over a time equal to the trap accumulation time. The inset depicts data at jet disruptor voltages of 260–290 V.
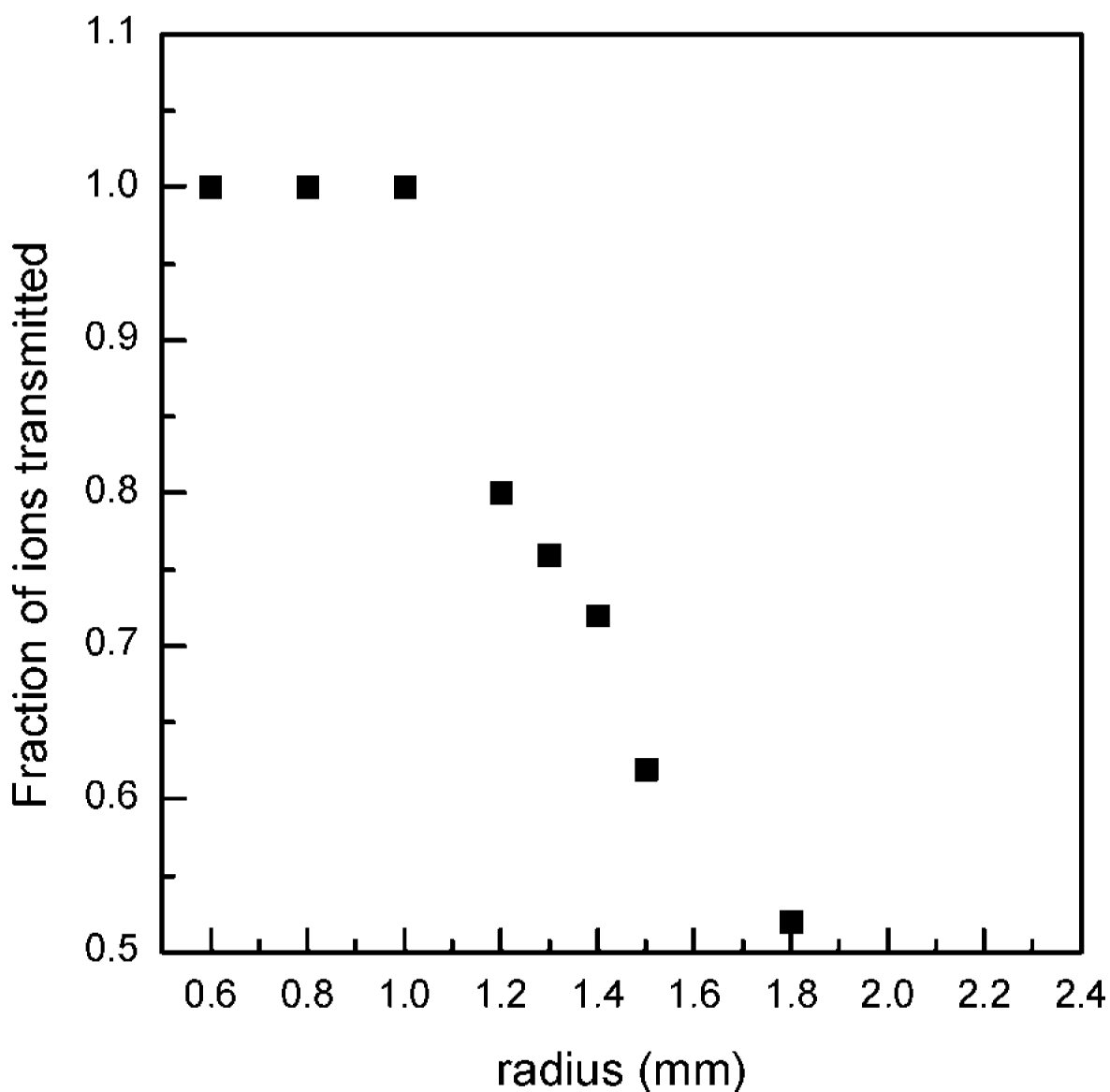
Figure 9.
Calculated number of triply charged neurotensin ions transmitted from the funnel exit electrode into the collisional quadrupole as a function of the ion beam radius. Data were obtained with SIMION 8.0. Each data point represents normalized transmission of 50 particles through the funnel/quadrupole interface. The gap between the ion funnel exit electrode and the collisional quadrupole rods was 1 mm. The estimated pressure in the gap was 100 mTorr. The collisional quadrupole rf voltage was 2.5 kV$_{pp}$.
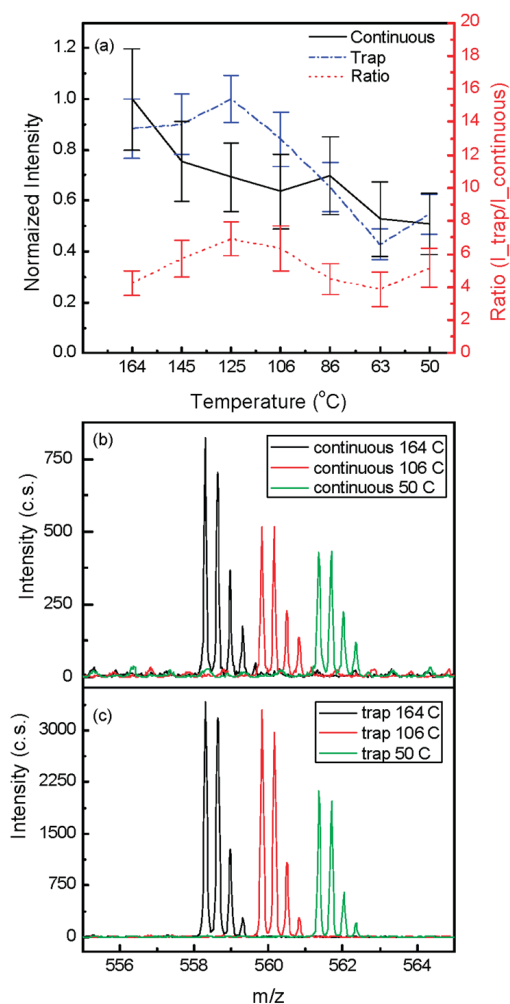
Figure 10.
(a) Normalized intensity for 10 nM triply charged neurotensin in the continuous and trapping (54 ms accumulation time) modes as a function of the heated capillary temperature. Portions of mass spectra for 10 nM triply charged neurotensin at three different heated capillary temperatures in (b) continuous mode and (c) trapping mode. The mass spectra are offset for clarity.

Table 1

Peptides Identified (within 10 ppm) from 0.05 *μ*g/*μ*L *S. oneidensis* Tryptic Digest, Using RPLC–MS in Both AGC-Trapping and Continuous Modes

monoisotopic mass	exptl *m/z*[a]	mass error (ppm)[b]	NET error[c]	peptide sequence
615.3591	308.6864	−1.61	0.0068	IDAGIK
702.3912	352.2061	9.09	0.0011	SLADIGK
731.4251	366.7199	0.30	0.0026	MELVLK
773.4283	387.7215	0.25	0.0095	NTTIPTK
785.4395	393.7263	−1.74	0.0169	LGDAVVGR
785.4395	393.7263	−1.74	0.0191	LGGAEIAR
785.4647	393.7415	4.90	0.0069	IQVAEVK
789.4054	395.7104	1.09	0.0006	AMGVDVAK
800.4643	401.2362	−8.01	0.0022	LDEAILK
810.4963	406.2542	−3.07	−0.0012	LIVVDPR
810.4963	406.2542	−3.07	−0.0012	IIVVDPR
816.4705	409.2407	−4.44	0.0046	SQVTGVVK
852.4163	427.2165	2.54	0.0084	LANYMNK
872.4967	437.2542	−3.23	−0.0144	VDASLAGIK
913.4868	457.7471	−7.88	0.0013	TTLTAAISH
913.4868	457.7471	−7.88	0.0094	GEINIPGSK
937.4868	469.7499	−1.68	−0.0141	GDLPAGSPKP
937.4981	469.7589	5.45	−0.0015	SKPHVNVGT
937.4981	469.7589	5.45	0.0116	AANHLEGVK
991.5086	496.7652	7.31	−0.0003	GIAGIDAYRG
991.5086	496.7652	7.31	0.0122	DGLYQQIR
1093.5767	547.7996	7.28	−0.0044	VSFTVTQGQK
1101.5778	551.7968	1.24	0.0024	STRGEVLAVGN
1101.5778	551.7968	1.24	0.0077	GAGSVLDEAKR
1103.5975	552.8045	−2.78	−0.0121	LVYNPAGSVGK
1152.5887	385.2016	−4.99	0.0001	NQADGLVHATK
1259.7085	630.8626	1.69	−0.0068	RIEAIVTTTEK
1295.6543	432.8919	−0.33	−0.0057	SLSAAVAYDMLR
1318.6802	660.3477	0.56	−0.0028	IEAAMSAVETAVK
1318.6880	660.3477	−5.40	−0.0037	FENAAVSVDVIR
1318.6880	660.3477	−5.40	0.0051	VIFDEVQTGVGR
1323.7186	662.8727	9.17	−0.0065	ISLVGFGTFEVR
1327.7499	443.5878	−6.22	0.0025	NGVLAGFPVLDVK
1342.6629	448.5624	1.94	−0.0049	DAQFERPDLPR
1416.7394	473.2566	6.12	−0.0083	MIADIKKDAQER
1416.7460	473.2566	1.51	−0.0025	EGVSKEEAEALKK
1433.7765	717.9009	7.50	0.0011	ALDSFIAAVTEGLK
1526.8052	764.4135	4.70	0.0017	AGDVDILVNNAGITR
1553.7561	518.9305	8.80	0.0001	SLSMVFSHAWHPR
1580.7946	527.9437	9.23	0.0011	RYQEGSEYPLIAR

monoisotopic mass	exptl m/z[a]	mass error (ppm)[b]	NET error[c]	peptide sequence
1580.8045	527.9437	2.97	−0.0131	VVEEAPAPGLSDELR
1580.8158	527.9437	−4.14	−0.0003	INDLGDASINAHLTK
1780.9332	594.6530	2.25	−0.0093	SKPHVNVGTIGHVDHGK
1929.9683	644.3252	−7.52	0.0000	VYHENKDVDVETLELK
2020.0476	674.3607	6.32	0.0028	GIALVATNGGSIKDYEGLDK
2177.2670	726.7655	3.48	−0.0020	ALIVTDKPLVNIGLVGEVAEK
2386.2525	796.4255	0.87	−0.0021	STKPQLPLVAINTTAGTASEMTR

[a] m/z of the most abundant charge state.

[b] Mass error from the AGC-trapping experiment.

[c] Error in normalized elution time (NET) (ref 28).